

Mathematical and Computer Modelling of Dynamical Systems

Methods, Tools and Applications in Engineering and Related Sciences

ISSN: 1387-3954 (Print) 1744-5051 (Online) Journal homepage: www.tandfonline.com/journals/nmcm20

Physics-based model of a lithium-ion battery cell in Modelica

Alfonso Urquía & Carla Martín-Villalba

To cite this article: Alfonso Urquía & Carla Martín-Villalba (2025) Physics-based model of a lithium-ion battery cell in Modelica, Mathematical and Computer Modelling of Dynamical Systems, 31:1, 2509513, DOI: [10.1080/13873954.2025.2509513](https://doi.org/10.1080/13873954.2025.2509513)

To link to this article: <https://doi.org/10.1080/13873954.2025.2509513>



© 2025 The Author(s). Published by Informa UK Limited, trading as Taylor & Francis Group.



Published online: 11 Jun 2025.



Submit your article to this journal [↗](#)



Article views: 400



View related articles [↗](#)



View Crossmark data [↗](#)

Physics-based model of a lithium-ion battery cell in Modelica

Alfonso Urquía and Carla Martín-Villalba

Departamento de Informática y Automática, Universidad Nacional de Educación a Distancia (UNED), Madrid, Spain

ABSTRACT

Electrochemical models of lithium-ion battery cells, such as the variants of the pseudo two-dimensional model proposed by Doyle, Fuller and Newman, find applications in cell design, diagnosis, and advanced model-based control, as these models allow to reproduce, over a wide range of experimental conditions, the current-voltage characteristics and the internal state of the cell. An implementation of this model and the most commonly employed analysis techniques, including current pulse trains, constant-current constant-voltage cycles, electrochemical impedance spectroscopy (EIS), and dynamic EIS, are presented. These models are organized into a novel Modelica library named *LilonCellP2D*, whose structure is discussed. A published model, developed by other authors, of a commercial lithium-ion cell manufactured by Kokam is used to illustrate the features of *LilonCellP2D*, and the simulation results are compared with those obtained using the Dandelion online simulator. *LilonCellP2D* was developed and tested using Dymola version 2024x.

ARTICLE HISTORY

Received 13 December 2024

Accepted 16 May 2025

KEYWORDS

Lithium-ion battery;
Modelica; pseudo-2D model;
DFN model

1. Introduction

Lithium-ion batteries are widely used in hybrid and electric vehicles, stationary energy storage systems, and portable electronics. A lithium-ion battery cell consists of two electrodes that are electronically insulated from each other by a separator, which allows the passage of ions but blocks the passage of electrons. Metallic current collectors are adhered at both ends of the electrodes, facilitating the conduction of electrons to the external circuit.

The cell electrodes and separator are porous materials, whose pores are filled with a liquid electrolyte that allows the transport of dissolved lithium ions. The porous structure of the electrodes increases the contact surface area between the solid and liquid phases. Electrolytes commonly consist of concentrated solutions of lithium salts dissolved in organic solvents, and additives.

The solid part of the electrodes consists of an active material that allows lithium intercalation in its crystalline structure; conductive materials that improve the

CONTACT Alfonso Urquía  aurquia@dia.uned.es  Departamento de Informática y Automática, Universidad Nacional de Educación a Distancia (UNED), Juan del Rosal 16, Madrid 28040, Spain

© 2025 The Author(s). Published by Informa UK Limited, trading as Taylor & Francis Group.

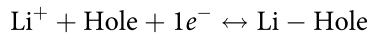
This is an Open Access article distributed under the terms of the Creative Commons Attribution License (<http://creativecommons.org/licenses/by/4.0/>), which permits unrestricted use, distribution, and reproduction in any medium, provided the original work is properly cited. The terms on which this article has been published allow the posting of the Accepted Manuscript in a repository by the author(s) or with their consent.

conductivity of the current carried by the electrons; and binders that enhance the structural stability of the electrodes.

The active material of the positive electrode (PE) is typically a lithium transition metal oxide, such as lithium iron phosphate, lithium manganese oxide, lithium cobalt oxide, and lithium nickel cobalt aluminium oxide. The active material of the negative electrode (NE) is commonly composed of graphite, silicon oxide, and lithium titanate. The separator does not contain any active material (i.e. lithium intercalation material). The current collector attached to the NE (NCC) is usually made of copper, and the current collector attached to the PE (PCC) is made of aluminium.

During cell discharge, neutral Li de-intercalates from the NE active material by releasing an electron and dissolves as Li^+ in the electrolyte. This charge transfer reaction takes place at the solid-electrolyte interface. Li^+ dissolved in the electrolyte is transported by diffusion and migration through the separator pores to the PE, where Li^+ gains an electron at the electrolyte-solid interface becoming neutral, and intercalates into the active material of the PE. To balance the charges, electrons circulate from NE to PE through the external circuit. This mechanism is reversed during cell charging.

The charge transfer reaction of the intercalation/de-intercalation process can be described as follows:



where Li^+ is the lithium ion that has arrived at the interfacial zone by diffusion in the electrolyte, Hole represents a hole without lithium in the active material, $1e^-$ is an electron that has arrived at the interfacial zone by conduction in the active material, and $\text{Li} - \text{Hole}$ represents a neutral lithium atom intercalated in the active material surface, ready to diffuse inside the active material. In addition to lithium transport and intercalation/de-intercalation, other processes take place that are responsible of cell ageing, by reducing cell capability to store and release energy. These degradation processes include side reactions that irreversibly reduce the amount of cyclable lithium and electrode structural damage caused by lithium intercalation.

Physics-based models of lithium-ion battery cells, commonly referred to as electrochemical models, find application in cell design, and advanced model-based control (Hariharan et al. 2018). Cell thermodynamics, charge transfer kinetics, and lithium transport are described from physical laws, allowing the current-voltage characteristics and internal state of the cell to be accurately reproduced over a wide range of experimental conditions. Degradation mechanisms can be accounted for in physics-based models, allowing a better understanding of the cell observable behaviour.

An influential physics-based model of the lithium-ion battery cell is the Doyle-Fuller-Newman (DFN) model (Doyle 1995; Doyle et al. 1993; Doyle and Newman 1995; Fuller et al. 1994), which is formulated on the basis of the so-called pseudo two-dimensional (P2D) approximation. According to the P2D approximation, lithium transport is described as two one-dimensional processes: the lithium-ion transport in the liquid electrolyte across the electrodes and separator; and the lithium diffusion in the solid active material of the electrodes. The latter is typically described as consisting of uniformly distributed particles with one of the following shapes (West et al. 1982):

parallel sheets, long cylinders, and spheres. In the DFN model, homogeneous spherical solid particles are considered at each point of the electrode to represent the active material. Lithium diffusion along the radial coordinate of each solid particle is described by Fick's law in spherical coordinates. Solid-phase diffusion of lithium between particles is neglected. The active material particles of an electrode are electrically connected, so that electrons can flow from any point of the active material to the corresponding current collector. Also, the electrolyte is assumed to be a continuum throughout the entire cell.

The DFN model describes the evolution of the lithium-ion concentration and electric potential in the liquid electrolyte that fills the pores of the electrodes and separator; and the lithium concentration and electric potential in the solid spherical particles of the active material. To this end, conservation laws of Li mass and electronic charge are imposed in the particles, and conservation laws of Li-ion mass and ionic charge are imposed in the electrolyte. The transport phenomena considered are migration and Fickian diffusion of Li-ions in the electrolyte; Fickian diffusion of lithium in the particles; Ohmic electron conduction in the solid part of the electrodes; and lithium intercalation/de-intercalation reaction at the particle–electrolyte interface.

Heat generation and transport are not considered in the DFN model. Nevertheless, cell operating temperature is typically taken into account when setting the value of those physical parameters whose value is strongly dependent on temperature, including electrolyte ionic conductivity, diffusivities of active material and electrolyte, and reaction rate constants.

Several DFN model extensions have been proposed to describe additional physical phenomena (Thomas et al. 2021), such as double-layer capacitance (Legrand et al. 2014), which is relevant on the milliseconds scale and thus can be neglected for current pulses with frequency less than 100 Hz (Ong and Newman 1999; Smith and Wang 2006), dynamic thermal behaviour (Srinivasan and Wang 2002), and degradation mechanisms (Arora et al. 1998; O'Kane et al. 2022; Ramadass et al. 2003).

An implementation in the Modelica language of a physics-based P2D model of lithium-ion battery cell is presented in this manuscript. The cell model and the supported analyses are structured as a Modelica library named *LiIonCellP2D*. The supported analyses include user-defined current pulse trains, which facilitate simulating pulsed current techniques, galvanostatic intermittent titration technique (GITT), and hybrid pulse power characterization (HPPC) test (US Department of Energy 2014); charge and discharge at constant current and constant voltage modes; and electrochemical impedance spectroscopy (EIS) and dynamic EIS (Lasia 2014).

Other approaches for the simulation of DFN model variants, and previous works aimed to facilitate the modelling of lithium-ion battery cells in Modelica, are described in Section 2. The modelling hypotheses, equations and the Modelica description of the cell model implemented in *LiIonCellP2D* are discussed in Sections 3 and 4, and the supported analyses in Section 5. Finally, the model of a commercial cell described in (Ecker et al. 2015; Ecker et al. 2015) is employed to illustrate some *LiIonCellP2D* features, and the simulation results are compared with those obtained for the same model by using the online Dandeliion simulator (Dandeliion Team 2024; Korotkin et al. 2021).

2. Related work

The DFN electrochemical model of the lithium-ion battery cell consists of a coupled set of nonlinear algebraic equations, and nonlinear partial differential equations with derivatives with respect to time and two spatial coordinates: the Cartesian x -coordinate along the cell thickness and the spherical r -coordinate along the particle radius. Different approaches are found in the literature for the simulation of the DFN model variants. Some authors employ modelling environments, such as COMSOL Multiphysics (Comsol 2024), that provide direct support for this type of mathematical model (i.e. partial differential algebraic equations and PDAE). Other authors apply a variety of techniques to discretize the spatial domain, transforming the model into a system of differential-algebraic equations (DAE) that can be simulated using a programming and numerical computing platform (e.g. Matlab) or numerical libraries written in programming languages such as FORTRAN, C++ or Python. Additionally, a number of dedicated simulation tools are available, including GT-SUITE/GT-AutoLion (Gamma Technologies 2024); the LIONSIMBA Matlab toolbox (Torchio et al. 2016); the Python package PyBaMM (Sulzer et al. 2021); and the Dandelion online simulator (Dandelion Team 2024; Korotkin et al. 2021).

Several authors have used Modelica to simulate the electrical and thermal behaviour of lithium-ion batteries, employing in most cases equivalent circuit models to represent the cell dynamics (Arianto et al. 2016; Dao and Schmitke 2015; Dvorak, Lacher, and Simic 2014; Gerl, Janczyk, and Krüger et al. 2014; Groß and Golubkov 2021; Maplesoft 2024; Modelon 2024a, 2024b; Pine and Choudhury 2020; Qin et al. 2019; Uddin and Picarelli 2014). For instance, the lithium-ion cell is modelled in (Arianto et al. 2016; Dvorak et al. 2014; Gerl et al. 2014; Uddin and Picarelli 2014) using an equivalent circuit model that consists of a voltage source whose value is the open circuit voltage of the cell, an internal resistance and two parallel resistor-capacitor circuits; whereas in (Qin et al. 2019) is modelled using three parallel resistor-capacitor circuits. The battery pack is composed in (Dvorak et al. 2014) by connecting 88 cell models in series.

Applications of the aforementioned Modelica models include battery load analysis and optimization, hardware-in-the-loop testing of battery management systems (BMS), thermal modelling and cooling system optimization to stabilize battery temperature, state-of-health effects on charge/discharge efficiency and thermal runaway, and battery ageing and degradation studies. The electrical parameter values of the equivalent circuit components depend on the state-of-charge (SOC), current and temperature, and are typically obtained from experimental measurements using numerical optimization techniques. For instance, battery cell parameters are estimated in (Arianto et al. 2016; Qin et al. 2019) carrying out a hybrid power pulse characterization (HPPC) test. In Gerl et al. (2014), ageing is accounted for by an ageing factor that depends on the number of cycles and the storage time of the battery, and it takes into account the power dissipation in the resistors of a cell and the heat transfer due to convection and radiation between cells within a package.

The DFN electrochemical model of the lithium-ion battery cell is described in Modelica, and implemented by using the MapleSim modelling and simulation tool, in (Dao and Schmitke 2015). The partial differential equations are approximated by applying the Galerkin's method, converting the PDE into a set of small in size, continuous

ordinary differential equations (ODEs), which is more numerically stable and faster to solve.

The modelling approach adopted in the *LiIonCellP2D* Modelica library is different. The DFN model, originally formulated as a PDAE, is converted into a DAE by discretizing the two spatial dimensions into control volumes, where mass and charge conservation are imposed. Spatial discretization does not hinder the physical interpretation of the model. Moreover, since the properties of the medium are delimited inside each control volume and the transport phenomena across each control plane can be specified individually, the analysis of spatial inhomogeneities, and spatially localized phenomena such as certain degradation mechanisms is facilitated.

3. Model description

In describing the model, the subscripts n , s and p are used to denote properties in the spatial domain of the NE, separator, and PE, respectively. For instance, the thicknesses of the NE, separator, and PE are denoted as L_n , L_s and L_p (units: m), respectively.

The system is discretized into control volumes along the two spatial dimensions of the P2D model: the x -coordinate, which spans across the cell thickness, and the r -coordinate of the spherical particles that represent the electrode active material. For the sake of clarity, the control volumes of the discretization along the x -coordinate are denoted as CV_x , and the control volumes of the discretization along the r -coordinate are denoted CV_r .

The origin of the x -coordinate is selected at the NCC-NE interface, as shown on the left in Figure 1. Therefore, the NCC-NE, NE-separator, separator-PE and PE-PCC interfaces are located at $x = 0$, $x = L_n$, $x = L_n + L_s$ and $x = L_n + L_s + L_p$, respectively. The electrode surface area (i.e. the area of the cell section perpendicular to the x -coordinate) is denoted as A_{cell} (units: m^2). The cell is discretized along the x -coordinate into CV_x : the NE, separator and PE into $N_{x,n}$, $N_{x,s}$ and $N_{x,p}$ CV_x respectively. This is done so that the CV_x of a given domain (NE, separator or PE) has the same length, which is generally different from the length of other domains. The total number of CV_x along the x -coordinate is $N_x = N_{x,n} + N_{x,s} + N_{x,p}$. The CV_x are numbered from 1 to N_x , starting with the CV_x of the NE that is adjacent to the NCC and finishing with the CV_x of the PE that is adjacent to the PCC. The length of the i -th CV_x is denoted as Δx_i , with $i = 1, \dots, N_x$, and is calculated as follows:

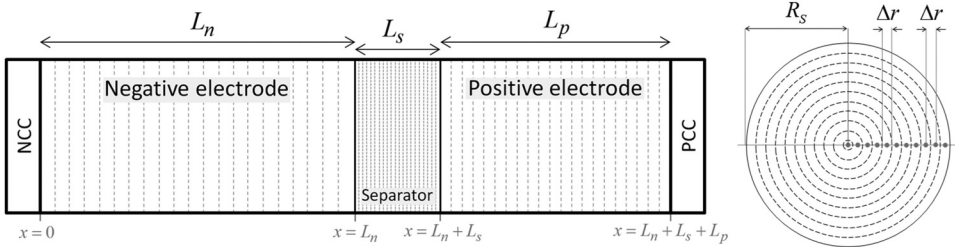


Figure 1. Discretizations into control volumes along the x (left) and r (right) coordinates.

$$\Delta x_i = \begin{cases} L_n/N_{x,n} & \text{for } i = 1, \dots, N_{x,n} \\ L_s/N_{x,s} & \text{for } i = N_{x,n} + 1, \dots, N_{x,n} + N_{x,s} \\ L_p/N_{x,p} & \text{for } i = N_{x,n} + N_{x,s} + 1, \dots, N_x \end{cases} \quad (1)$$

Each CV_x comprises a portion of the cell's porous material. The properties of the active material and the electrolyte are of interest in the CV_x of the electrodes, and the properties of the electrolyte are of interest in the CV_x of the separator. The parameters ε_L and ε_S (unitless) indicate the volume fraction of the CV_x occupied by the electrolyte (the L subscript stands for liquid), and by the active material (the S subscript stands for solid), respectively.

It is assumed that the properties and state (Li^+ concentration and electric potential) of the electrolyte contained within each CV_x are spatially homogeneous. It is also assumed that the electrolyte is electrically neutral: cation and anion concentrations in the electrolyte are the same in each CV_x .

As in the DFN model, solid-diffusion of lithium in the active material of the electrodes is modelled by considering that the active material consists of a number of homogeneous spherical particles, each one completely surrounded by electrolyte. If all spherical particles contained in each CV_x are assumed to be equal, then the number of particles per CV_x is calculated by dividing the volume of the active material contained in the CV_x ($\varepsilon_{S,i} \cdot A_{\text{cell}} \cdot \Delta x_i$ for the i -th CV_x) by the particle volume. In general, different types of active material particles, characterized by different values of the diffusion coefficient and radius, can be considered in the CV_x . For instance, blended electrodes (e.g. silicon-graphite NE) can be modelled assuming that each CV_x contains solid spheres of different types: one per component. The number of particles of each type present in each CV_x is calculated as previously described, but taking into account the volume fraction of each active material component in the CV_x . Assuming that all the particles of each type, contained in the same CV_x , are in the same initial state and all undergo the same processes, only the lithium diffusion in one particle of each type needs to be simulated per CV_x . For the sake of simplicity, hereafter it is assumed that there is only one type of active material particle per CV_x in the electrodes.

Lithium conservation and diffusion within each spherical solid particle is described by discretizing the solid particle into N_r control volumes (denoted as CV_r) as follows: an inner sphere of radius $\Delta r/2$ and concentric spherical shells, each of thickness $\Delta r = R_S/(N_r - 0.5)$, where R_S (units: m) is the particle radius (see the right side of [Figure 1](#)). The volumes $v_{S,i}$ (units: m^3) of the CV_r , and the areas $S_{S,i}$ (units: m^2) of the adjacent control planes (CP_r) are:

$$v_{S,1} = \frac{4}{3} \cdot \pi \cdot r_{S,1}^3, \quad v_{S,i} = \frac{4}{3} \cdot \pi \cdot (r_{S,i}^3 - r_{S,i-1}^3) \quad \text{for } i = 2, \dots, N_r \quad (2)$$

$$S_{S,i} = 4 \cdot \pi \cdot r_{S,i}^2 \quad \text{for } i = 1, \dots, N_r \quad (3)$$

where

$$r_{S,i} = \Delta r \cdot (i - 0.5) \quad \text{for } i = 1, \dots, N_r \quad (4)$$

The lithium concentration inside the i -th CV_r is $c_{S,i}$ (units: $\text{mol} \cdot \text{m}^{-3}$). Lithium diffusion between adjacent CV_r is described by Fick's law. The diffusion coefficient of

lithium in the i -th CV_r , $D_{S,i}$ (units: $\text{m}^2 \cdot \text{s}^{-1}$), depends strongly on the lithium stoichiometry, defined as the quotient of the actual lithium concentration and its maximum value ($\chi = \frac{c_s}{c_{s,max}}$, unitless) and temperature.

The diffusive molar flow rate per surface unit from the i -th to the $(i + 1)$ -th CV_r , $j_{S,i}$ (units: $\text{mol} \cdot \text{m}^{-2} \cdot \text{s}^{-1}$), is calculated as follows:

$$j_{S,i} = 2 \cdot \frac{D_{S,i} \cdot D_{S,i+1}}{D_{S,i} + D_{S,i+1}} \cdot \frac{c_{S,i} - c_{S,i+1}}{\Delta r} \quad \text{for } i = 1, \dots, N_r - 1 \quad (5)$$

Lithium mass balance is posed inside each CV_r :

$$v_{S,1} \cdot \frac{dc_{S,1}}{dt} = -S_{S,1} \cdot j_{S,1} \quad (6)$$

$$v_{S,i} \cdot \frac{dc_{S,i}}{dt} = S_{S,i-1} \cdot j_{S,i-1} - S_{S,i} \cdot j_{S,i} \quad \text{for } i = 2, \dots, N_r - 1 \quad (7)$$

$$v_{S,N_r} \cdot \frac{dc_{S,N_r}}{dt} = S_{S,N_r-1} \cdot j_{S,N_r-1} - S_{S,N_r} \cdot j_{tc} \quad (8)$$

The lithium concentration at the particle outer CV_r , c_{S,N_r} , is denoted as $c_{S,sup}$ (units: mol/m^3). The lithium stoichiometry at the particle outer surface, χ_{sup} (unitless), is calculated by dividing $c_{S,sup}$ by the maximum lithium concentration in the active material, $c_{s,max}$ (units: mol/m^3).

$$\chi_{sup} = \frac{c_{S,sup}}{c_{s,max}} \quad (9)$$

The total number of lithium moles in a particle, M_r (units: mol), is calculated as follows:

$$M_r = \sum_{i=1}^{N_r} c_{S,i} \cdot v_{S,i} \quad (10)$$

The total number of moles of lithium diffused in the active material of the i -th CV_x , $M_{x,i}$ (units: mol), is calculated by multiplying the number of solid particles in the CV_x by the total number of moles per particle:

$$M_{x,i} = \frac{\varepsilon_{S,i} \cdot \Delta x_i \cdot A_{cell}}{4/3 \cdot \pi \cdot R_{S,i}^3} \cdot M_{r,i} \quad (11)$$

The total number of moles of lithium diffused in the active material of an electrode is calculated by adding the moles diffused in all the CV_x of the electrode. The state-of-charge (SOC) of each electrode is calculated by dividing the actual number of moles diffused in the electrode's active material by its maximum value, which is calculated by multiplying the active material volume by the maximum lithium concentration allowed in the active material ($c_{s,max}$).

The molar flow rate of lithium from the particle outer surface to the surrounding electrolyte, per unit surface area, j_{tc} (units: $\text{mol} \cdot \text{m}^{-2} \cdot \text{s}^{-1}$), is calculated from the Butler–Volmer equation:

$$j_{ic} = j_0 \cdot \left[\exp\left(\frac{\alpha_a \cdot F}{R_G \cdot T} \cdot \eta\right) - \exp\left(-\frac{\alpha_c \cdot F}{R_G \cdot T} \cdot \eta\right) \right] \quad (12)$$

where F is the Faraday's constant ($96485.33289 \text{ C} \cdot \text{mol}^{-1}$), α_a (unitless) and α_c (unitless) are the charge transfer coefficients, R_G is the perfect gas constant ($8.314 \text{ J} \cdot \text{K}^{-1} \cdot \text{mol}^{-1}$), T (units: K) is the absolute temperature, η (units: V) is the surface overpotential that drives the reaction, and j_0 (units: $\text{mol} \cdot \text{m}^{-2} \cdot \text{s}^{-1}$) is given by:

$$j_0 = k \cdot c_L^{\alpha_a} \cdot (c_{S,max} - c_{S,sup})^{\alpha_a} \cdot c_{S,sup}^{\alpha_c} \quad (13)$$

where c_L (units: $\text{mol} \cdot \text{m}^{-3}$) is the lithium-ion concentration in the electrolyte, and k (units: $\text{m}^{2.5} \cdot \text{mol}^{-0.5} \cdot \text{s}^{-1}$) is the constant of transfer velocity of electrochemical charge.

The total molar flow rate from a solid particle is calculated as j_{ic} times the outer surface area of the particle. In each CV_x , the total molar flow rate of lithium from the active material to the electrolyte can be calculated by adding the contributions of all the solid particles contained in the CV_x . By dividing by the volume of the CV_x , the total molar flow per unit of volume of the CV_x , F_{ic} (units: $\text{mol} \cdot \text{m}^{-3} \cdot \text{s}^{-1}$), can be calculated.

The electric currents associated with these molar flows can be calculated by multiplying the molar flow rate by the Faraday's constant. The electric current associated with the lithium intercalation/de-intercalation within the i -th CV_x of an electrode is denoted as $I_{ic,i}$ (units: A), for $i = 1, \dots, N_n, N_n + N_s + 1, \dots, N_x$, and it can be calculated as shown below. This current is positive as it flows from the active material to the electrolyte (i.e. lithium de-intercalation).

$$I_{ic,i} = F \cdot j_{ic,i} \cdot \frac{3 \cdot \varepsilon_{S,i}}{R_{S,i}} \cdot \Delta x_i \cdot A_{cell} \quad (14)$$

The mass conservation law can be applied, in every CV_x , to the lithium ion dissolved in the electrolyte. Lithium-ion transport by diffusion and migration takes place across the control planes (CP_x) between adjacent CV_x . Additionally, in the CV_x of the electrodes, there is lithium-ion consumption/generation by the charge transfer reaction of intercalation/de-intercalation to/from the active material. The mass conservation of lithium ion dissolved in the electrolyte is formulated as follows:

$$\varepsilon_{L,1} \cdot \frac{dc_{L,1}}{dt} = -\frac{J_1}{\Delta x_1} + (1 - t^+) \cdot F_{ic,1} \quad (15)$$

$$\varepsilon_{L,i} \cdot \frac{dc_{L,i}}{dt} = \frac{J_{i-1} - J_i}{\Delta x_i} + (1 - t^+) \cdot F_{ic,i} \quad \text{for } i = 2, \dots, N_n \quad (16)$$

$$\varepsilon_{L,i} \cdot \frac{dc_{L,i}}{dt} = \frac{J_{i-1} - J_i}{\Delta x_i} \quad \text{for } i = N_n + 1, \dots, N_n + N_s \quad (17)$$

$$\varepsilon_{L,i} \cdot \frac{dc_{L,i}}{dt} = \frac{J_{i-1} - J_i}{\Delta x_i} + (1 - t^+) \cdot F_{ic,i} \quad \text{for } i = N_n + N_s + 1, \dots, N_x - 1 \quad (18)$$

$$\varepsilon_{L,N_x} \cdot \frac{dc_{L,N_x}}{dt} = \frac{J_{N_x-1}}{\Delta x_{N_x}} + (1 - t^+) \cdot F_{tc,N_x} \quad (19)$$

where $c_{L,i}$ (units: $\text{mol} \cdot \text{m}^{-3}$) is the lithium ion concentration in the electrolyte of the i -th CV_x , and J_i (units: $\text{mol} \cdot \text{m}^{-2} \cdot \text{s}^{-1}$) is the molar flow of lithium ion transported by diffusion through the CP_x that separates the i -th and $(i+1)$ -th CV_x (see Figure 2).

$$c_{L,i} - c_{L,i+1} = J_i \cdot \left(\frac{0.5 \cdot \Delta x_i}{D_{\text{eff},i}} + \frac{0.5 \cdot \Delta x_{i+1}}{D_{\text{eff},i+1}} \right) \text{ for } i = 1, \dots, N_x - 1 \quad (20)$$

The second term on the right-hand side of Equations (15, 16, 18 and 19) describes the intercalation/de-intercalation of lithium in the active material of the electrodes, and the lithium-ion migration. The transference number t^+ expresses the fraction of current carried by Li^+ in the electrolyte.

$D_{\text{eff},i}$ is the effective diffusivity of lithium-ion in the electrolyte contained in the i -th CV_x . It is typically expressed as the product of a permeability factor $B_{L,i}$ (unitless), and the diffusivity of Li^+ in the bulk electrolyte solution $D_{L,i}$ (units: $\text{m}^2 \cdot \text{s}^{-1}$).

$$D_{\text{eff},i} = B_{L,i} \cdot D_{L,i} \quad (21)$$

Some authors describe the permeability factor as $B_{L,i} = \varepsilon_{L,i}^b$, where the b coefficient is known as the Bruggeman factor. The bulk diffusivity $D_{L,i}$ typically depends on the electrolyte composition, lithium-ion concentration, and temperature.

The total number of lithium-ion moles in the electrolyte, M_L (units: mol), is calculated by adding the contribution of all CV_x :

$$M_L = A_{\text{cell}} \cdot \sum_{i=1}^{N_x} \varepsilon_{L,i} \cdot \Delta x_i \cdot c_{L,i} \quad (22)$$

Electric charge does not accumulate in the CV_x . In every CV_x , at any time, the total input current is equal to the total output current, and is equal to the current I_{cell} (units: A) flowing through the external circuit. Electric current is caused by the flow of electrons in the active material and by the flow of ions in the electrolyte. Since an electric current is associated with the charge transfer reaction that takes place in the CV_x of the electrodes, the proportion of current transmitted by electrons and ions varies from one CP_x to

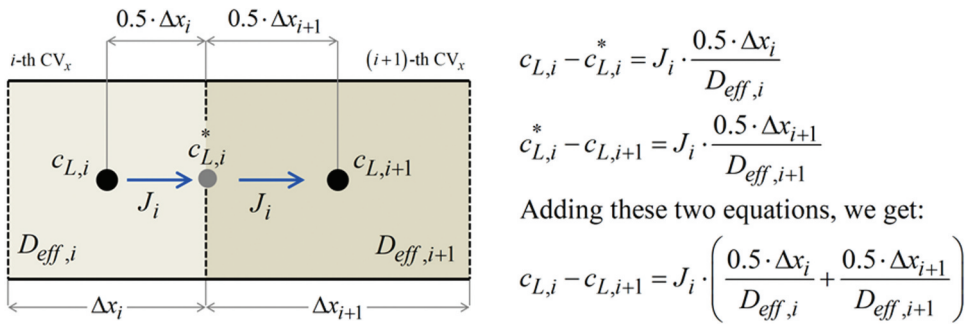


Figure 2. Molar flow of lithium ion transported by diffusion through the CP_x that separates the i -th and $(i+1)$ -th CV_x .

another in the electrodes. In the separator, since it contains no active material, the current is completely conducted by ions transported in the electrolyte. In the current collectors, the charge carriers are electrons.

The cell current I_{cell} is considered positive when it leaves the positive terminal of the battery cell. The I_{cell} current flows into the NCC from the external circuit, and enters the active material of the first CV_x , where the charge carriers are electrons. Inside the cell, the I_{cell} current is due to the flow of electrons in the solid material and ions in the electrolyte. The I_{cell} current, carried by electrons, leaves the active material of the N_x -th CV_x , passing through the PCC to the external circuit.

It is assumed that the active material and the electrolyte contained in each CV_x are two equipotential volumes. The variables $\phi_{L,i}$ with $i = 1, \dots, N_x$ represent the potential of the electrolyte, and $\phi_{S,i}$ with $i = 1, \dots, N_n, N_n + N_s + 1, \dots, N_x$ the potential of the active material.

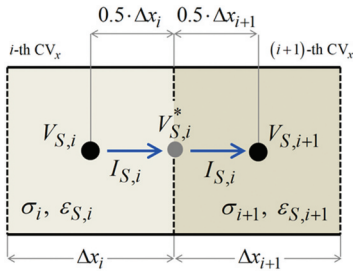
The rate of the charge transfer reaction taking place in the CV_x of the electrodes, as described in Equation (12), depends on the overpotential η between the active material and the electrolyte. This overpotential quantifies the difference between the local electric potential, $V_{S,i} - V_{L,i}$ (potential of the active material minus electrolyte potential, both in the i -th CV_x), and the equilibrium potential $V_{OCP,i}$.

$$\eta_i = V_{S,i} - V_{L,i} - V_{OCP,i} \text{ for } i = 1, \dots, N_n, N_n + N_s + 1, \dots, N_x \quad (23)$$

The equilibrium potential ($V_{OCP,i}$) depends on the lithium stoichiometry at the particle outer surface (χ_{sup}).

Ohm's law is applied to calculate the electron current between adjacent CV_x , which is conducted in the active material (see Figure 3). $I_{S,i}$ (units: A) represents the electric current caused by the flow of electrons in the solid material, from the i -th to the $(i + 1)$ -th CV_x , through the CP_x that separates them. $I_{S,0}$ represents the current flowing from the external circuit to the first CV_x , and I_{S,N_x} the current flowing to the external circuit from the last CV_x . The electron current does not flow through the separator. The electron conductivity of the bulk active material, σ_i (units: $S \cdot m^{-1}$), depends on the composition and temperature of the active material.

$$I_{S,i} \cdot \frac{1}{2 \cdot A_{cell}} \cdot \left(\frac{\Delta x_i}{\varepsilon_{S,i} \cdot \sigma_i} + \frac{\Delta x_{i+1}}{\varepsilon_{S,i+1} \cdot \sigma_{i+1}} \right) = V_{S,i} - V_{S,i+1} \quad (24)$$



$$V_{S,i} - V_{S,i}^* = I_{S,i} \cdot \frac{0.5 \cdot \Delta x_i}{A_{cell} \cdot \varepsilon_{S,i} \cdot \sigma_i}$$

$$V_{S,i}^* - V_{S,i+1} = I_{S,i} \cdot \frac{0.5 \cdot \Delta x_{i+1}}{A_{cell} \cdot \varepsilon_{S,i+1} \cdot \sigma_{i+1}}$$

Adding these two equations, we get:

$$V_{S,i} - V_{S,i+1} = I_{S,i} \cdot \left(\frac{0.5 \cdot \Delta x_i}{A_{cell} \cdot \varepsilon_{S,i} \cdot \sigma_i} + \frac{0.5 \cdot \Delta x_{i+1}}{A_{cell} \cdot \varepsilon_{S,i+1} \cdot \sigma_{i+1}} \right)$$

Figure 3. Ohm's law is applied to calculate the electron current conducted in the active material through the CP_x that separates the i -th and $(i + 1)$ -th CV_x .

for $i = 1, \dots, N_n - 1, N_n + N_s + 1, \dots, N_x - 1$.

Analogously, $I_{L,i}$ (units: A) represents the electric current caused by the flow of ions in the electrolyte, from the i -th to the $(i + 1)$ -th CV_x , through the CP_x that separates them. A modification of Ohm's law, commonly referred to as the MacInnes' Equation (Bizeray 2016, p. 26), allows to calculate this current:

$$I_{L,i} \cdot \frac{1}{2 \cdot A_{cell}} \cdot \left(\frac{\Delta x_i}{\kappa_{eff,i}} + \frac{\Delta x_{i+1}}{\kappa_{eff,i+1}} \right) = V_{L,i} - V_{L,i+1} + 2 \cdot (1 - t^+) \cdot \frac{R_G \cdot T}{F} \cdot (\log(c_{L,i+1}) - \log(c_{L,i})) \quad (25)$$

for $i = 1, \dots, N_x - 1$, where $\kappa_{eff,i}$ (units: $S \cdot m^{-1}$) is the effective ionic conductivity in the electrolyte contained in the i -th CV_x , which quantifies the facility of an electric field to transport lithium ions. It is calculated as the product of the permeability factor $B_{L,i}$ (unitless) and the ionic conductivity in the bulk electrolyte ($\kappa_{L,i}$), which depends on the lithium-ion concentration, and temperature.

$$\kappa_{eff,i} = B_{L,i} \cdot \kappa_{L,i} \quad (26)$$

The left-hand side and the first two terms on the right-hand side of Equation (25) correspond to Ohm's law. The third term accounts for the overpotential induced by variations in the ionic concentration in the electrolyte.

Summarizing the previous discussion (see Figure 4), the electric current flowing through the CP_x that interface with the CC is:

$$I_{cell} = I_{S,0} = I_{S,N_x} \quad (27)$$

$$0 = I_{L,0} = I_{L,N_x} \quad (28)$$

The current balance in the CV_x of the electrodes is:

$$I_{S,i-1} = I_{S,i} + I_{tc,i} \quad (29)$$

$$I_{L,i-1} + I_{tc,i} = I_{L,i} \quad (30)$$

For $i = 1, \dots, N_n, N_n + N_s + 1, \dots, N_x$. The current thought the CP_x in the NE-separator interface is:

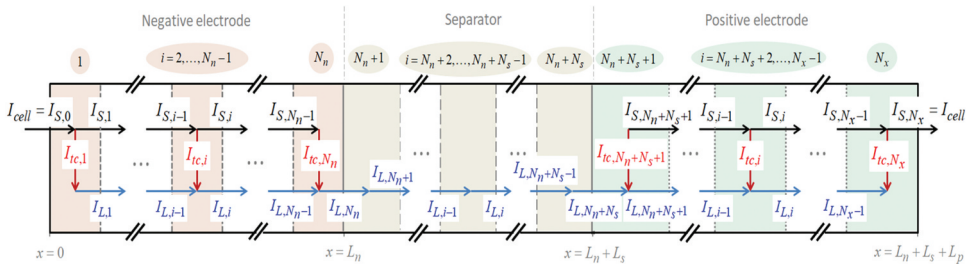


Figure 4. Electric current flowing through the cell.

$$I_{S,N_n} = 0 \quad (31)$$

The current through the CP_x of the separator is:

$$I_{L,i} = I_{cell} \quad (32)$$

for $i = N_n + 1, \dots, N_n + N_s$. Since the separator does not contain any active material, $I_{S,i}$ is not defined for $i = N_n + 1, \dots, N_n + N_s$.

The cell terminal voltage V_{cell} is calculated from the potential of the active material contained in the CV_x adjacents to the charge collectors, excluding the ohmic drop due to the resistance R_{ctc} of the NCC-NE and PE-PCC connections:

$$V_{cell} = V_{S,N_x} - V_{S,1} - R_{ctc} \cdot I_{cell} \quad (33)$$

4. Cell model implementation in Modelica

The top-level packages of the *LiIonCellP2D* Modelica library are shown in Figure 5a. These are the *Device*, *Analyses*, *Catalogue* and *Examples* packages, whose content is shown in Figure 5b–e. The model of the lithium-ion cell is structured into the *Device* package (see Figure 5b), as described below.

The *SolidSphere* class describes the lithium diffusion and conservation in the spherical particles of active material. The particle radius (R_s), the maximum concentration of lithium ($c_{S,max}$) and the number of CV_r (N_r) are class parameters whose values are set by the modeller. From these parameters, the CV_r volumes and CP_r surface areas are calculated as described by Equations (2) and (3). The diffusive molar flow rate per area unit, as described by Equation (5), the lithium mass balance in the CV_r , as described by Equations (6–8), and the total number of lithium moles in the particle, as described by Equation (10), are calculated.

By default, the lithium concentration is assumed to be initially the same in all CV_r and equal to a value provided by the modeller (as customary in Modelica, these initial conditions can be modified when defining the experiment). The diffusion coefficient in each CV_r is a function of the lithium stoichiometry in the CV_r (e.g. $c_{S,i}/c_{S,max}$ in the i -th

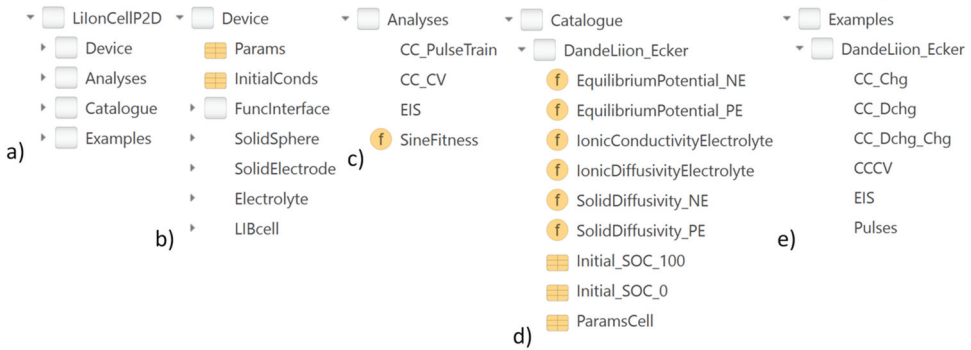


Figure 5. *LiIonCellP2D* Modelica library: (a) Top-level packages; and (b–e) *Device*, *Analyses*, *Catalogue* and *Examples* packages.

CV_r). This relationship is described by a replaceable function whose input is the lithium stoichiometry and whose output is the diffusion coefficient.

The *SolidElectrode* class describes the active material of an electrode. Two instances of this class are used to describe the NE and PE. The number of CV_x ($N_{x,n}$ or $N_{x,p}$, for NE or PE respectively) is a parameter whose value is set by the modeller. Also, the electrode thickness (L_n or L_p), the cross-sectional area of the cell (A_{cell}), the electron conductivity in the bulk material (σ), and the volume fraction of the active material (ε_s) are parameters set by the modeller. The CV_x length is calculated according to Equation (1). An array of components of the *SolidSphere* class describes the lithium diffusion and conservation in the active material: one component of the array is associated with each CV_x . The modeller is allowed to set, for each component, the corresponding values of the particle radius, the maximum lithium concentration, and the number of CV_r , and to specify the function describing the solid diffusivity.

The *SolidElectrode* class contains the Ohm's law, as described by Equation (24), that relates the current and voltage in the active material; the Equation (29) that imposes the current conservation in the active material; and Equation (14) that relates j_{ic} and I_{ic} . The total number of moles of lithium intercalated in the active material of the electrode is calculated by adding the contributions of all the CV_x of the electrode, which are calculated as described in Equation (11).

The *Electrolyte* class describes the entire electrolyte. The separator thickness (L_s) and the number of CV_x into which the separator is discretized ($N_{x,s}$) are set by the modeller. The CV_x length in the separator is calculated according to Equation (1). The electrode lengths (L_n and L_p), and number of CV_x ($N_{x,n}$ and $N_{x,p}$) are the same as specified by the modeller when defining the two instances of the *SolidElectrode* class. The total number of CV_x is calculated by adding the number of CV_x of each of the three domains: $N_x = N_{x,n} + N_{x,s} + N_{x,p}$. The quantities that define the electrolyte state and properties, such as lithium-ion concentration and voltage, are declared as vector variables with N_x components (one component per CV_x). The mass conservation and modified Ohm's laws are imposed, as described by Equations (15–19), and Equation (25). The temperature intervenes explicitly in Equation (25). Since the presented model does not account for heat generation and transport, temperature is a parameter whose value needs to be provided by the modeller. The lithium-ion diffusion through CP_x in the electrolyte is described using a vector variable with $N_x - 1$ components, and Equation (20) relates these flows with their driving concentrations. The total number of lithium-ion moles in the electrolyte is calculated as described by Equation (22). Two replaceable functions are employed to calculate the ionic electrical conductivity and the ionic diffusivity in the bulk electrolyte, as a function of the lithium-ion concentration. The effective ionic conductivity and diffusivity are calculated as described in Equations (26 and 21), respectively. The permeability factor is a vector parameter with N_x components (one per CV_x).

The *LIBcell* class defines the battery cell. Two instances of the *SolidElectrode* class describe the active material of the two electrodes, and one instance of the *Electrolyte* class describes the electrolyte. The modeller needs to specify the functions to calculate the solid diffusivity (D_s) of the NE and PE in terms of the lithium stoichiometry; and the ionic conductivity (κ_L) and diffusivity (D_L) of the bulk electrolyte in terms of the lithium-ion molar concentration.

The physical phenomenon that connects the electrode and electrolyte models is the charge transfer reaction, which is described by the Butler–Volmer equation applied to each CV_x of the electrodes. The reaction is driven by the overpotential between the active material and the electrolyte, described by Equations (23). The equilibrium potential of the active material intervenes in this equation. Two replaceable functions (one per electrode) are employed to calculate the equilibrium potential, in terms of the lithium stoichiometry at the outer surface of the active material particle. Additionally, the cell voltage is calculated as described by Equations (33), and the boundary conditions for the electronic current in the active material described by Equations (27) and (31) are imposed.

The following parameters are declared in the *LIBcell* class: the operating temperature (T), and the parameters that define the spatial discretization of the micro- and macro-spatial domains ($N_{x,n}$, $N_{x,s}$ and $N_{x,p}$; $N_{r,n}$ and $N_{r,p}$). The charge transfer coefficients of the Butler–Volmer equation are set to the values $\alpha_a = \alpha_c = 0.5$.

The declaration of the following 21 cell parameters is grouped in a record class named *Params*: area of the cell section perpendicular to the x -coordinate (A_{cell}); thicknesses of NE, separator and PE (L_n , L_s and L_p); NE and PE particle radii ($R_{S,n}$ and $R_{S,p}$); volume fraction of active material in NE and PE ($\varepsilon_{S,n}$ and $\varepsilon_{S,p}$); electron conductivity of the bulk active material in NE and PE (σ_n and σ_p); maximum lithium concentration in NE and PE ($c_{S,max,n}$ and $c_{S,max,p}$); porosity of NE, separator and PE ($\varepsilon_{L,n}$, $\varepsilon_{L,s}$ and $\varepsilon_{L,p}$); transference number of electrolyte (t^+); permeability factor of NE, separator and PE ($B_{L,n}$, $B_{L,s}$ and $B_{L,p}$); and constant of transfer velocity of electrochemical charge in NE and PE (k_n and k_p).

A record class named *InitialConds* is declared to facilitate the model initialization by specifying the initial lithium-ion concentrations in the electrolyte of NE, separator and PE; the initial lithium concentrations in the active material of NE and PE; the initial voltages of the active material of NE and PE; and the initial voltage of the electrolyte. Subclasses of this record class can be defined, and passed as parameters to the instance of the *LIBcell* class.

5. Analysis implementation in Modelica

The *Analyses* package of *LiIonCellP2D* (see Figure 5c) contains partial models defining the following three types of analyses: an arbitrary sequence of current pulses; constant current and constant voltage charging and discharging; and electrochemical impedance spectroscopy (EIS). The current supplied to or provided by the battery cell (I_{cell}) is calculated from these classes for the corresponding analysis type, as explained below. The following sign convention is adopted in the analysis classes: positive current values discharge the battery, while negative values charge it. The cell voltage and state are calculated from the battery cell model (i.e. an instance of the *LIBcell* class).

The *CC_PulseTrain* partial model has a two-dimensional matrix parameter that allows to specify the pulse train by means of time-current pairs of values. For instance, the values $\{0,0\}$, $\{100,0.5\}$, $\{1100,0\}$, $\{1200,-0.5\}$, $\{2200,0\}$ indicate that the current equals zero in the interval $[0,100]$ s, at time 100 s undergoes a fast, continuous change to the 0.5 A value, keeps this value in the interval $[100 + \delta, 1100]$ s, at time 1100 s undergoes a fast, continuous change to the zero value, keeps this value in

the interval $[1100 + \delta, 1200]$ s, at time 1200 s undergoes a fast, continuous change to the -0.5 A value, keeps this value in the interval $[1200 + \delta, 2200]$ s, at time 2200 s undergoes a fast, continuous change to the zero value, and keeps this value indefinitely. The continuous changes at the pulse steps are exponential in shape, and the transitions take a time well below the time scale of the phenomena considered in the battery cell model.

The *CC_CV* partial model describes a configurable number of cycles, each consisting of the following step sequence: rest (i.e. $I_{cell} = 0$), charge at constant current until the cell voltage reaches a target value, maintain this voltage until the cell current gets below a cut-off value, rest, discharge at constant current until the cell voltage gets below a target value, maintain this voltage until the cell current is below a cut-off value, and rest. The constant voltage step is implemented by manipulating the cell current using an integral control strategy. All current changes are continuous to facilitate numerical simulation. As with the *CC_PulseTrain* analysis, the time constants are well below the time scale of the battery cell model.

The *EIS* partial model implements electrochemical impedance spectroscopy (EIS), and dynamic EIS analyses. An array parameter defines the test frequencies. For each test frequency w , the cell impedance is calculated. The following sign convention is used for cell current in the EIS analysis: current entering the positive electrode (which occurs during charging) is considered positive. A sinusoidal current, superposed to a constant value, is forced.

$$I_{cell} = I_{0,DC} + I_{0,AC} \cdot \sin(w \cdot (t - t_{start})) \quad (34)$$

This input current is kept for a predefined number of cycles set by the modeller. During the last cycle, a predefined number of cell voltage (V_{cell}) readings are automatically made at equispaced sampling instants. The average of these readings is calculated and subtracted to the readings. From these voltage-time pairs, $\tilde{V}_{cell} - t$, the least square method is applied to calculate the best-fitting \tilde{V}_{amp} and \tilde{V}_{phase} parameters of the function:

$$\tilde{V}_{cell} = \tilde{V}_{amp} \cdot \sin(w \cdot (t - t_{start}) + \tilde{V}_{phase}) \quad (35)$$

The impedance modulus and phase at the w frequency are $\tilde{V}_{amp}/I_{0,AC}$ and \tilde{V}_{phase} , respectively. This calculation procedure is automatically applied to the test frequencies in sequence, allowing a rest period of configurable duration between consecutive frequencies, during which $I_{cell} = I_{0,DC}$. The analysis results (i.e. test frequencies and their corresponding impedances in Cartesian and polar forms) are written to the log window using the *print* function included in the *Streams* package of the Modelica Standard Library. The simulation finishes automatically by calling the *terminate* Modelica function when all the test frequencies have been simulated. The modeller simply needs to set a simulation stop time long enough to allow for the analysis to be executed to completion.

6. Case of use

The physics-based model of a lithium-ion cell manufactured by Kokam, described in Ecker, Tran et al. (2015); Ecker, Käbitz et al. (2015), is used to illustrate the capabilities of *LiIonCellP2D*. Furthermore, as the Dandeliion online simulator (Dandeliion Team

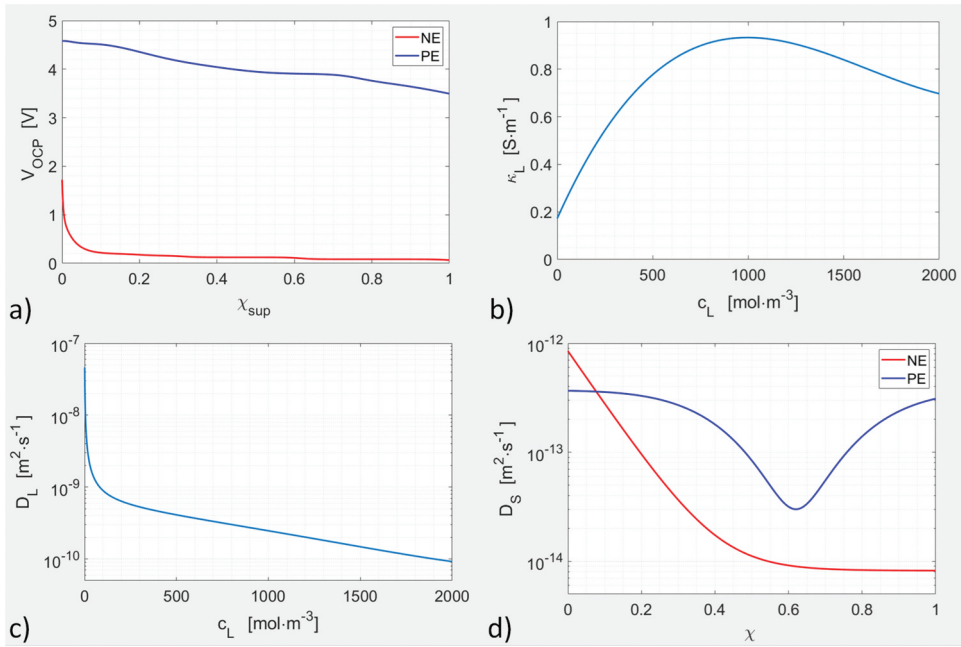


Figure 6. Cell parameters defined as functions (Dandelion Team 2024): a) equilibrium potentials of the NE and PE, as functions of the lithium stoichiometry at the particle outer surface, $V_{OCP,NE} = 0.7165 \cdot \exp(-369.03 \cdot \chi_{sup}) + 0.1219 \cdot \exp(-35.648 \cdot (\chi_{sup} - 0.053095)) - 0.018919 \cdot \tanh(21.197 \cdot (\chi_{sup} - 0.19618)) - 0.016964 \cdot \tanh(27.137 \cdot (\chi_{sup} - 0.31283)) - 0.019931 \cdot \tanh(28.57 \cdot (\chi_{sup} - 0.61422)) - 0.93115 \cdot \exp(36.328 \cdot (\chi_{sup} - 1.1074)) + 0.14003$, $V_{OCP,PE} = -2.3521 \cdot \chi_{sup} - 0.074706 \cdot \tanh(31.886 \cdot (\chi_{sup} - 0.021992)) + 6.3498 \cdot \tanh(2.664 \cdot (\chi_{sup} - 0.17435)) - 0.64024 \tanh(5.4862 \cdot (\chi_{sup} - 0.43925)) - 3.8238 \cdot \tanh(4.1217 \cdot (\chi_{sup} - 0.17619)) - 0.054212 \cdot \tanh(18.292 \cdot (\chi_{sup} - 0.76227)) + 4.2329$; b) ionic electrical conductivity of the bulk electrolyte calculated as a third-degree polynomial of the lithium-ion concentration [Ecker, Tran et al., 2015 Eq. (1)], $\kappa_L = 0.2667 \cdot 10^{-9} \cdot c_L^3 - 1.2983 \cdot 10^{-6} \cdot c_L^2 + 1.7919 \cdot 10^{-3} \cdot c_L + 0.1726$; c) ionic diffusivity of the bulk electrolyte calculated from the Einstein relation [Ecker et al. 2015, Eq. (3)], $D_L = 2.646 \cdot 10^{-7} \cdot (0.2667 \cdot 10^{-9} \cdot c_L^3 - 1.2983 \cdot 10^{-6} \cdot c_L^2 + 1.7919 \cdot 10^{-3} \cdot c_L + 0.1726) / c_L$; and d) diffusivities of lithium in the electrode active materials calculated as functions of lithium stoichiometry, $D_{S,NE} = 8.4 \cdot 10^{-13} \cdot \exp(-11.3 \cdot \chi) + 8.2 \cdot 10^{-15}$, $D_{S,PE} = 3.7 \cdot 10^{-13} - 3.4 \cdot 10^{-13} \cdot \exp(-12 \cdot (\chi - 0.62)^2)$.

2024; Korotkin et al. 2021) provides an implementation of this model, the simulation results obtained using *LiIonCellP2D* and *Dandelion* can be compared.

The model parameters are defined in the *Dandelion_Ecker* package, included within the *Catalogue* package of *LiIonCellP2D* (see Figure 5d). The parameters defined as functions are represented in Figure 6. The battery is composed of 48 sheets, each of which is described by the following parameters (Dandelion Team 2024; Ecker et al. 2015): $A_{cell} = 85.85 \cdot 10^{-4} \text{ m}^2$, $L_n = 74 \cdot 10^{-6} \text{ m}$, $L_s = 20 \cdot 10^{-6} \text{ m}$, $L_p = 54 \cdot 10^{-6} \text{ m}$, $R_{S,n} = 13.7 \cdot 10^{-6} \text{ m}$, $R_{S,p} = 6.5 \cdot 10^{-6} \text{ m}$, $\varepsilon_{S,n} = 0.3724$, $\varepsilon_{S,p} = 0.4083$, $\sigma_n = 14 \text{ S} \cdot \text{m}^{-1}$, $\sigma_p = 68.1 \text{ S} \cdot \text{m}^{-1}$, $c_{S,max,n} = 31920 \text{ mol} \cdot \text{m}^{-3}$, $c_{S,max,p} = 48580 \text{ mol} \cdot \text{m}^{-3}$, $\varepsilon_{L,n} = 0.329$, $\varepsilon_{L,s} = 0.508$, $\varepsilon_{L,p} = 0.296$, $t^+ = 0.26$, $B_{L,n} = 0.1620$, $B_{L,s} = 0.3040$,

$B_{L,p} = 0.1526$, $k_n = 2.3330 \cdot 10^{-10} \text{ m}^{2.5} \cdot \text{mol}^{-0.5} \cdot \text{s}^{-1}$ and $k_p = 0.59 \cdot 10^{-10} \text{ m}^{2.5} \cdot \text{mol}^{-0.5} \cdot \text{s}^{-1}$.

The simulations discussed in this section start with the cell fully charged. In this initial state (specified in the *Initial_SOC_100* record shown in Figure 5d), the concentrations are $C_{L,n} = C_{L,s} = C_{L,p} = 10^3 \text{ mol} \cdot \text{m}^{-3}$, $C_{S,n} = 26120 \text{ mol} \cdot \text{m}^{-3}$, $C_{S,p} = 12631 \text{ mol} \cdot \text{m}^{-3}$; and the initial values employed in *LiIonCellP2D* for voltage iteration are $V_{S,n} = 0$, $V_{S,p} = 4.182$ and $V_L = -0.084 \text{ V}$. The *Dandelion_Ecker* package contained within the *Examples* package (see Figure 5e) gathers the classes that describe the simulation experiments.

The *LiIonCellP2D* simulations presented in this section have been performed using Dymola 2024x, dassl algorithm with tolerance 10^{-5} , 500 output intervals, and Advanced. SparseActivate = true (Dassault Systèmes AB 2023). To evaluate the trade-off between spatial discretization error and simulation CPU time, the following eight spatial discretizations $\{N_{x,n}, N_{x,s}, N_{x,p}, N_{r,n}, N_{r,p}\}$ of the *LiIonCellP2D* models are compared: $\{21, 21, 21, 21, 21\}$, $\{31, 9, 23, 31, 15\}$, $\{31, 31, 31, 31, 31\}$, $\{41, 11, 31, 41, 21\}$, $\{41, 41, 41, 41, 41\}$, $\{51, 15, 37, 51, 25\}$, $\{61, 17, 45, 61, 29\}$ and $\{51, 51, 51, 51, 51\}$. The spatial discretization method selected in Dandelion is Finite Elements and Control Volumes (2nd order), and unless otherwise specified, the number of nodes in the electrolyte and solid particles is the default: 30/20/30 nodes in the electrolyte along the x-coordinate of the NE/separator/PE, and 30 nodes along the radial coordinate in the solid particles of NE and PE.

The simulation results saved to file by Dandelion and Dymola are analysed and plotted using Matlab. Dandelion generates several text files with a header and columns of numbers separated by spaces. In these files, Dandelion logs the evolution of the cell current and voltage, the evolution of the voltage at selected x positions of the solid and the electrolyte, the evolution of the lithium ion concentration at selected x positions of the electrolyte, and the evolution of the lithium concentration of selected positions along the radial coordinate of the solid particles located at five equidistant points along the x coordinate in each electrode ($x_{rel} = 0, 0.25, 0.5, 0.75, 1$). Dymola stores the evolution of all the model variables in a single .mat file.

6.1. Discharge and charge at constant current

Battery discharge and charge at three constant currents is simulated with Dandelion and *LiIonCellP2D*, and the results are compared. The battery nominal capacity is 7.5 Ah. The battery currents considered are C/48 (i.e. $7.5/48 = 0.15625 \text{ A}$), which allows to obtain a pseudo open-circuit voltage, 1C (i.e. 7.5 A), and 4C (i.e. $4 \cdot 7.5 = 30 \text{ A}$). As the parameter values correspond to only one sheet and the complete battery contains 48 sheets, the simulated current corresponds to one forty-eighth of the battery current. The charge, nominal, and discharge voltage values specified by the cell manufacturer are 4.2, 3.7 and 2.7 V, respectively.

The cell voltage simulated using Dandelion, and *LiIonCellP2D* with $\{51, 51, 51, 51, 51\}$ spatial discretization, are shown in the upper parts of Figures 7–9. In the same plots, the percentage errors of the *LiIonCellP2D* cell voltages with respect to the Dandelion cell voltages are plotted in green. Additionally, to evaluate the convergence of the

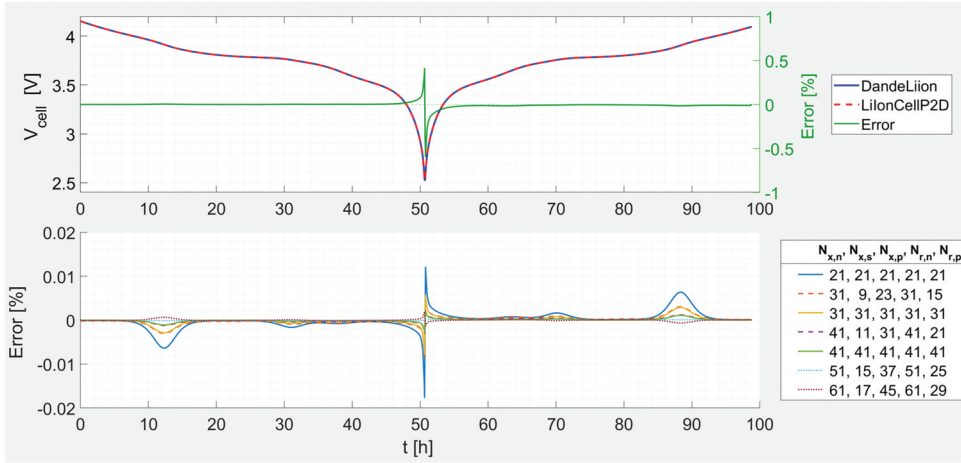


Figure 7. Steps: rest 1 s, CC DChg C/48, rest 300 s, CC Chg C/48, rest 300 s. StopTime: 355700 s. I_{cell} is specified as the pulse train $\{\{0, 0\}, \{1, I_{C48}\}, \{182300, 0\}, \{182600, -I_{C48}\}, \{355400, 0\}\}$.

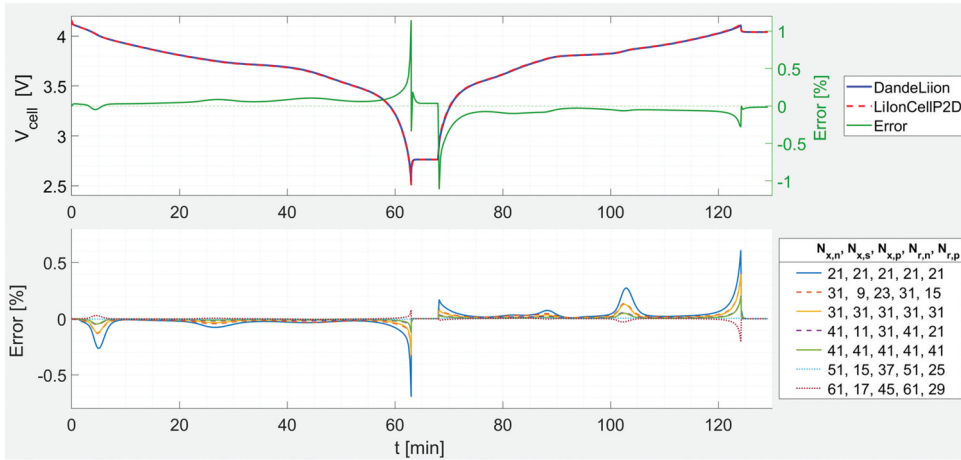


Figure 8. Steps: rest 1 s, CC DChg 1C, rest 300 s, CC Chg 1C, rest 300 s. StopTime: 7750 s. I_{cell} is specified as the pulse train $\{\{0, 0\}, \{1, I_{1C}\}, \{3780, 0\}, \{4080, -I_{1C}\}, \{7450, 0\}\}$.

LilonCellP2D spatial discretization, the percentage errors in cell voltage of the other seven discretizations with respect to $\{51, 51, 51, 51, 51\}$ are shown in the lower parts of Figures 7–9. To complete the data required to achieve a trade-off between simulation accuracy and speed, the number of equations and the simulation CPU times are given in columns 6–9 of Table 1.

As a further example of the validations that have been performed, the concentrations calculated using DandeLiion and *LilonCellP2D* are compared. The evolution during the discharge and charge at 4C (performed as described in Figure 9) of the lithium ion

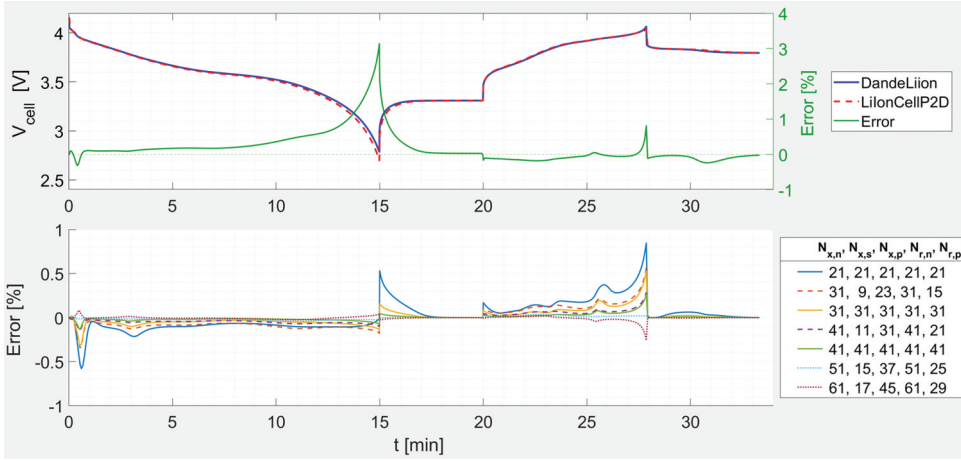


Figure 9. Steps: rest 1 s, CC DChg 4C, rest 300 s, CC Chg 4C, rest. StopTime: 2000s. I_{cell} is specified as the pulse train $\{\{0, 0\}, \{1, I_{4C}\}, \{899, 0\}, \{1199, -I_{4C}\}, \{1672, 0\}\}$. DandeLiion: 50/40/50 nodes in electrolyte, and 60 nodes in solid particles.

Table 1. Data for performance analysis of LilonCellP2D simulations.

Spatial discretization						CPU time ^a (s)					
						DChg Chg @ CC			Pulses		
						C/48	1C	4C	1C	4C	CCCV
$N_{x,n}$	$N_{x,s}$	$N_{x,p}$	$N_{r,n}$	$N_{r,p}$	# equations ^b						
21	21	21	21	21	3534	0.43	0.53	0.84	2.07	0.91	1.32
31	9	23	31	15	4926	0.74	0.89	1.55	3.44	1.54	2.04
31	31	31	31	31	7064	1.07	1.33	2.27	5.21	2.30	3.22
41	11	31	41	21	8324	1.58	1.88	3.36	7.29	3.20	4.31
41	41	41	41	41	11,794	2.37	2.71	4.74	10.6	4.61	6.46
51	15	37	51	25	12,206	2.69	3.23	5.93	12.4	5.38	7.10
61	17	45	61	29	17,026	4.60	5.28	9.98	20.3	8.85	11.6
51	51	51	51	51	17,724	4.30	5.05	8.84	19.2	8.48	11.4

^aCPU time (units: s) for integration using Dymola 2024x installed on Microsoft Windows 11 and a Lenovo ThinkPad with an 11th Gen Intel Core i9. ^bNumber of equations in the CC_DChg_Chg and Pulses models. The number of equations for the CCCV model is slightly larger.

concentration in the electrolyte, and the lithium concentration in the solid particles are shown in Figures 10 and 11, respectively.

6.2. Electrodes with particles of different radii

The *LiIonCellP2D* cell model allows the particle radius in each CV_x of each electrode to be specified independently as a model parameter. DandeLiion allows to divide each electrode along the x coordinate into two regions with different particle radii. The boundary between the regions is specified by giving its relative x -coordinate, x_R . Relative x -coordinates are normalized for each electrode with respect to its length so that the electrode spans from $x_{rel} = 0$ to $x_{rel} = 1$. Two particle radius multipliers, R_{left} and R_{right} , and a nominal particle radius R_S , are defined for each electrode. The radius of the

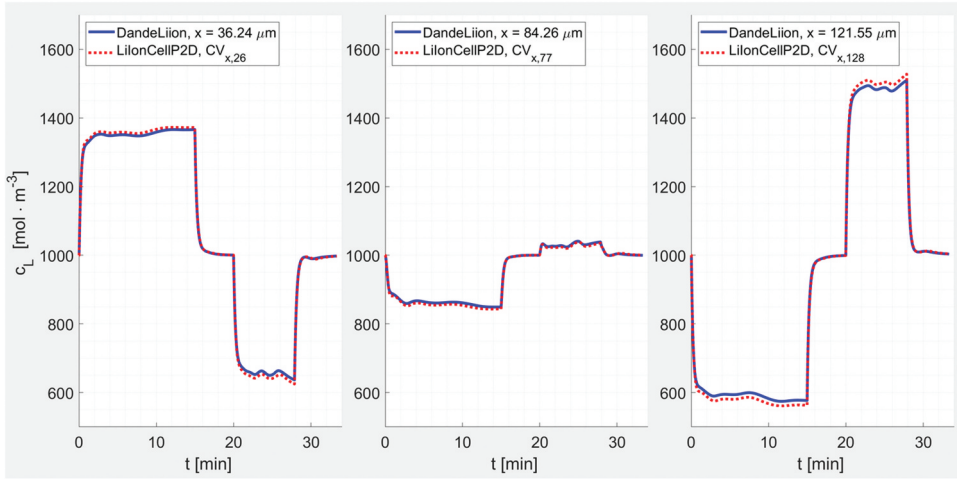


Figure 10. Lithium ion concentration in the electrolyte during discharge and charge at 4C, as described in Figure 9. As the spatial discretization of *LilonCellP2D* model is $\{51, 51, 51, 51, 51\}$, $CV_{x,26}$, $CV_{x,77}$ and $CV_{x,128}$ are located in the centre of the NE, separator, and PE, respectively.

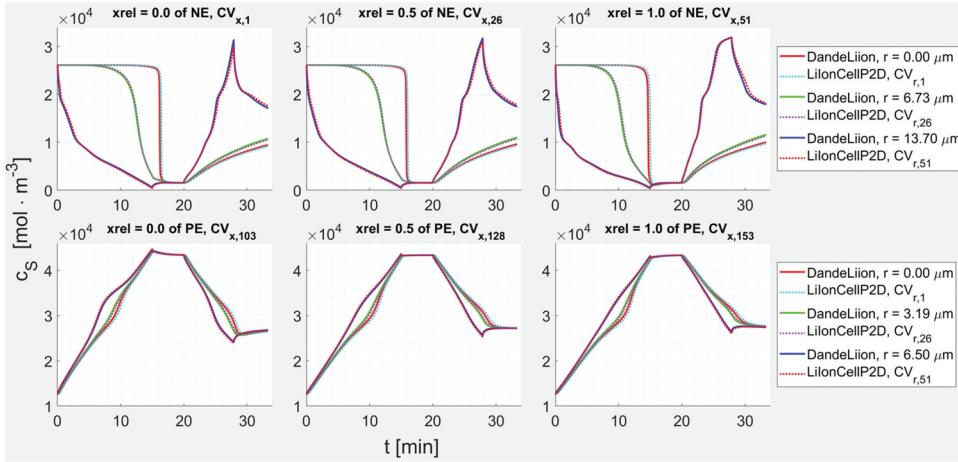


Figure 11. Lithium concentration in solid particles of NE (three plots in the top row) and PE (three plots in the bottom row) during discharge and charge at 4C, as described in Figure 9. The spatial discretization of the *LilonCellP2D* model is $\{51, 51, 51, 51, 51\}$. The plots in the first, second and third columns correspond to CV_x located in the leftmost ($CV_{x,1}$ and $CV_{x,103}$), middle ($CV_{x,26}$ and $CV_{x,128}$) and rightmost ($CV_{x,51}$ and $CV_{x,153}$) parts of the electrodes, respectively. Each plot represents the lithium concentration at three positions inside the solid particle: at the centre ($CV_{r,1}$), at half the radius ($CV_{r,26}$), and at the surface of the sphere ($CV_{r,51}$).

particles in the region $x_{rel} \in [0, x_R]$ is $R_{left} \cdot R_S$, and the radius in the region $x_{rel} \in (x_R, 1]$ is $R_{right} \cdot R_S$.

Two different particle sizes are defined in each electrode. The boundary between the regions in the NE and PE is defined by $x_{rel} = 2/3$ and $x_{rel} = 1/3$ respectively

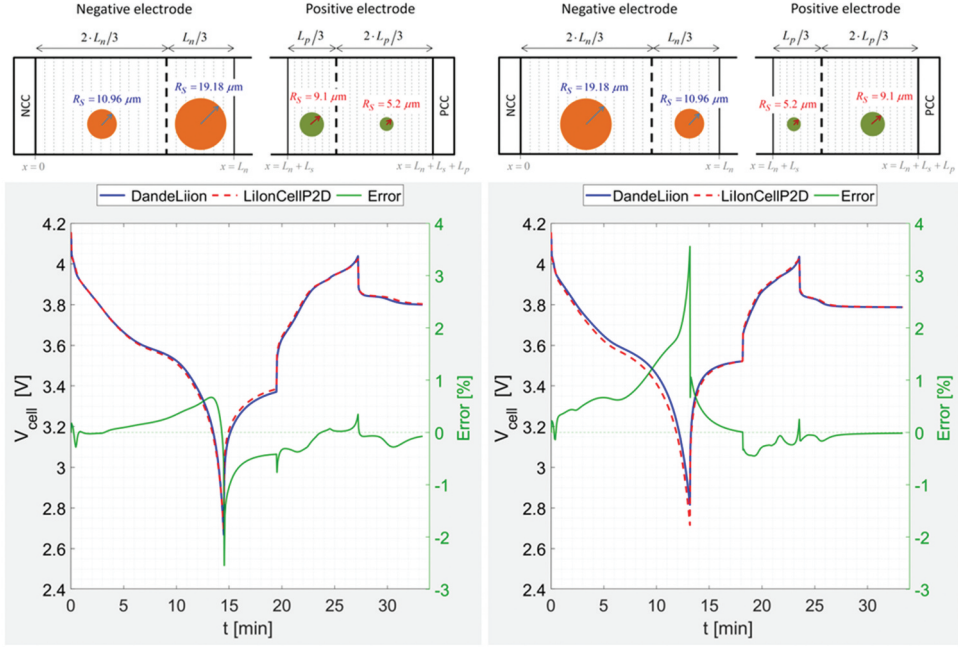


Figure 12. $x_{rel} = 2/3$ in NE and $x_{rel} = 1/3$ in PE. $R_{S,n} = 13.7 \cdot 10^{-6}$ m, $R_{S,p} = 6.5 \cdot 10^{-6}$ m. The spatial discretization of the *LilonCellP2D* model is $\{51, 51, 51, 51, 51\}$. Simulation stop time: 2000s. Case 1 (left): Particle radius multipliers: $\{R_{left}, R_{right}\} = \{0.8, 1.4\}$ in NE and $\{1.4, 0.8\}$ in PE. I_{cell} is specified as the pulse train $\{0, 0\}, \{1, I_{4C}\}, \{869, 0\}, \{1169, -I_{4C}\}, \{1633, 0\}$; CPU time of *LilonCellP2D* simulation: 6.72 s; Dandelion: 30/20/30 nodes in the electrolyte along the x-coordinate of the NE/separator/PE, and 30 nodes along the radial coordinate in the solid particles of NE and PE. Case 2 (right): Particle radius multipliers: $\{1.4, 0.8\}$ in NE and $\{0.8, 1.4\}$ in PE. I_{cell} is specified as the pulse train $\{0, 0\}, \{1, I_{4C}\}, \{790, 0\}, \{1090, -I_{4C}\}, \{1412, 0\}$; CPU time of *LilonCellP2D* simulation: 6.60 s; Dandelion: 50/40/50 nodes in the electrolyte along the x-coordinate of the NE/separator/PE, and 60 nodes along the radial coordinate in the solid particles of NE and PE.

(see top row of Figure 12). Two different sets of radii are simulated. In the first case, the NE particle radius multipliers are $\{R_{left}, R_{right}\} = \{0.8, 1.4\}$, and the PE particle radius multipliers are $\{1.4, 0.8\}$. In the second case, the NE and PE particle radius multipliers are $\{1.4, 0.8\}$ and $\{0.8, 1.4\}$, respectively. The cells are discharged and charged at 4C constant current, allowing them to rest after each constant current step (see the caption of Figure 12). The cell voltages obtained by simulation with *LiIonCellP2D* and Dandelion are plotted in the bottom row of Figure 12. The relative error of the *LiIonCellP2D* cell voltage with respect to the Dandelion voltage is plotted in green.

6.3. Discharge using periodic current pulses

Cell discharge by periodic current pulses of amplitudes 1C and 4C is simulated using Dandelion and *LiIonCellP2D*. The pulse period is 300 s. The simulations end when the cell voltage goes below 2.5 V. The cell voltage simulated using Dandelion, and

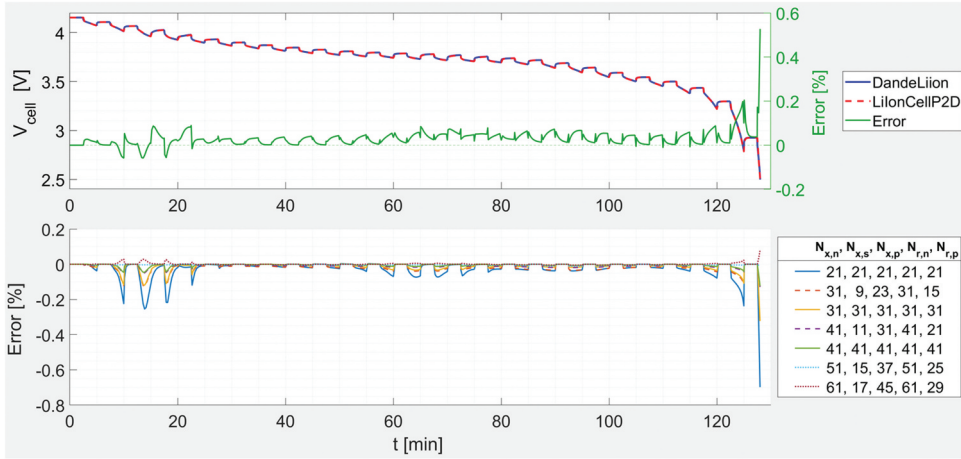


Figure 13. Cell discharge by periodic current pulses of amplitude 1C and period 300 s: I_{cell} is specified as the pulse train $\{0, 0\}, \{150, I_{1C}\}, \{300, 0\}, \{450, I_{1C}\}, \{600, 0\}, \dots\}$. DandeLiion: maximum time step of 0.1 s; 50/40/50 nodes in electrolyte, and 50 nodes in solid particles.

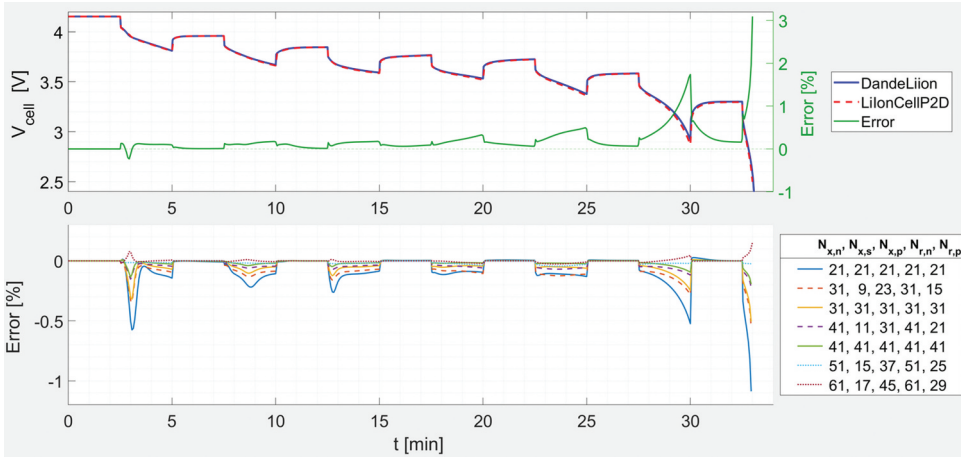


Figure 14. Cell discharge by periodic current pulses of amplitude 4C and period 300 s: I_{cell} is specified as the pulse train $\{0, 0\}, \{150, I_{4C}\}, \{300, 0\}, \{450, I_{4C}\}, \{600, 0\}, \dots\}$. DandeLiion: 30/20/30 nodes in electrolyte, and 30 nodes in solid particles.

LiIonCellP2D with $\{51, 51, 51, 51, 51\}$ spatial discretization, are shown in the upper parts of Figures 13 and 14, where the percentage errors of the *LiIonCellP2D* cell voltages with respect to the DandeLiion cell voltages are plotted in green. The percentage errors in cell voltage of the other seven discretizations with respect to $\{51, 51, 51, 51, 51\}$ are shown in the lower parts of Figures 13 and 14. The simulation CPU times of the *LiIonCellP2D* models are shown in columns 10 and 11 of Table 1.

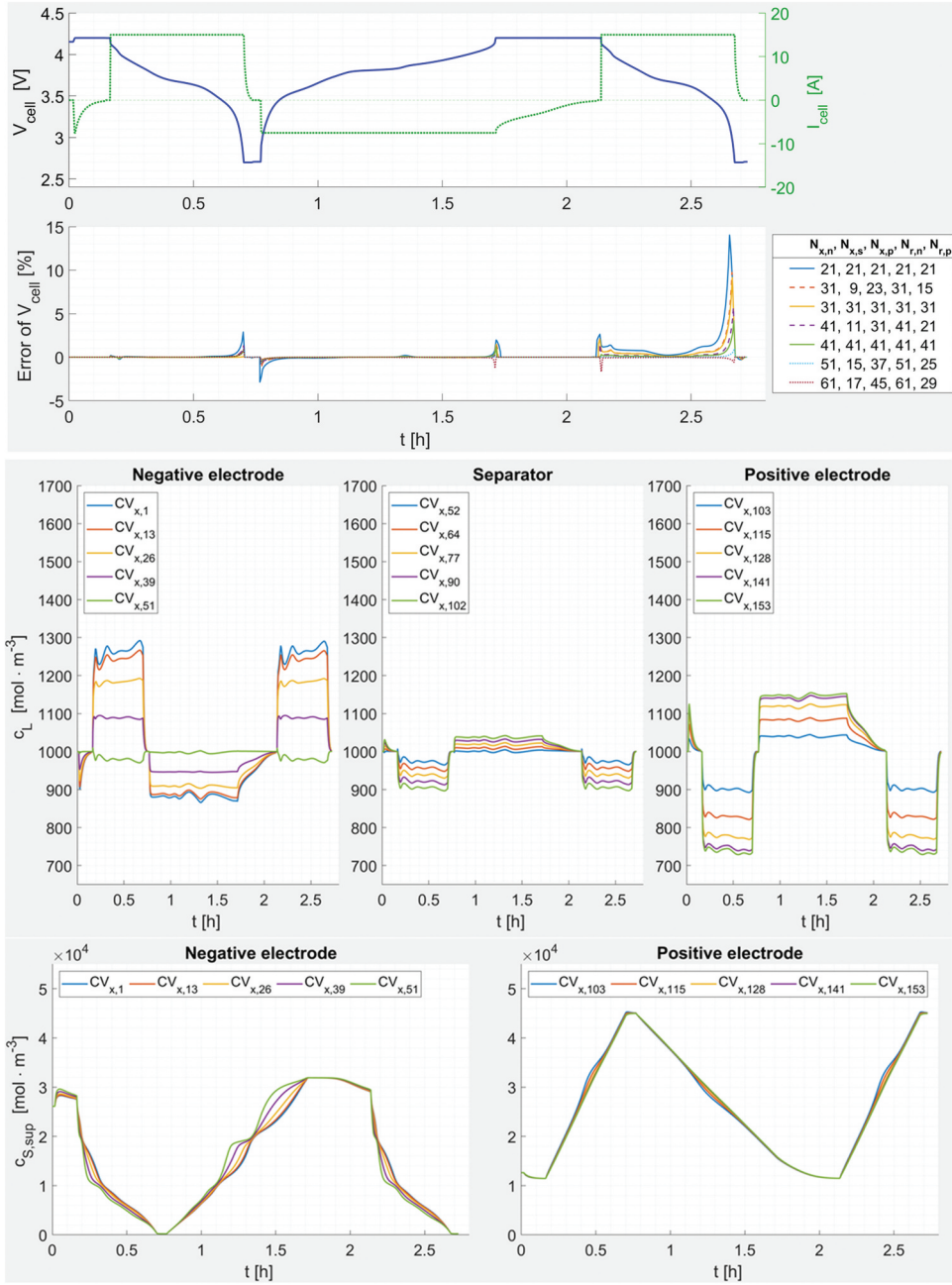


Figure 15. *LilonCellP2D* simulation results of the following test: rest 60s; CC-CV Chg 1C, voltage 4.2 V, cut-off current C/40; rest 60s; CC-CV Dchg 2C, cut-off voltage 2.7 V, cut-off current C/40; rest 120 s; CC-CV Chg 1C, voltage 4.2 V, cut-off current C/40; rest 60s; CC-CV Dchg 2C, cut-off voltage 2.7 V, cut-off current C/40; and rest 60s.

6.4. Charge and discharge at constant current–constant voltage

LiIonCellP2D facilitates to simulate sequences of charge and discharge cycles performed with a constant current–constant voltage (CC-CV) strategy. This example is intended to illustrate this feature. The selected charging and discharging currents coincide with those approved by the battery manufacturer: 1C and 2C, respectively. The test steps are indicated in the caption of Figure 15, where the following results are plotted: the cell current and voltage simulated using *LiIonCellP2D* with {51, 51, 51, 51, 51} spatial discretization, the percentage errors of the cell voltage of the other seven spatial discretizations with respect to {51, 51, 51, 51, 51}, and the lithium ion concentration in the electrolyte and the lithium concentration in the solid within some selected CV_x. The simulation CPU time corresponding to each of the eight *LiIonCellP2D* spatial discretizations is given in the last column of Table 1.

6.5. Electrochemical impedance spectroscopy

The EIS analysis performed on a fully charged cell is simulated in the frequency range from 1 mHz to 100 Hz using *LiIonCellP2D*. To facilitate the numerical simulation, the test frequencies are grouped according to their order of magnitude, and an independent EIS analysis is simulated for each group of frequencies. Five frequency groups are defined: {100, 90, ..., 20, 10} Hz, {10, 9, ..., 2, 1} Hz, {1, 0.9, ..., 0.2, 0.1} Hz, {0.1, 0.09, ..., 0.02, 0.01} Hz and {0.01, 0.009, ..., 0.001} Hz. The simulation of the lowest and highest frequencies of the groups is duplicated to check the consistency of the simulations. The sinusoidal input current is maintained for 10 cycles at each test frequency, and 20 readings are taken at equidistant sampling times during the last cycle, which are used to calculate the cell impedance at that frequency. The stop time of the simulations performed on these frequency groups is in the order of 3, 30, 300, 3000 and 30000 s, respectively.

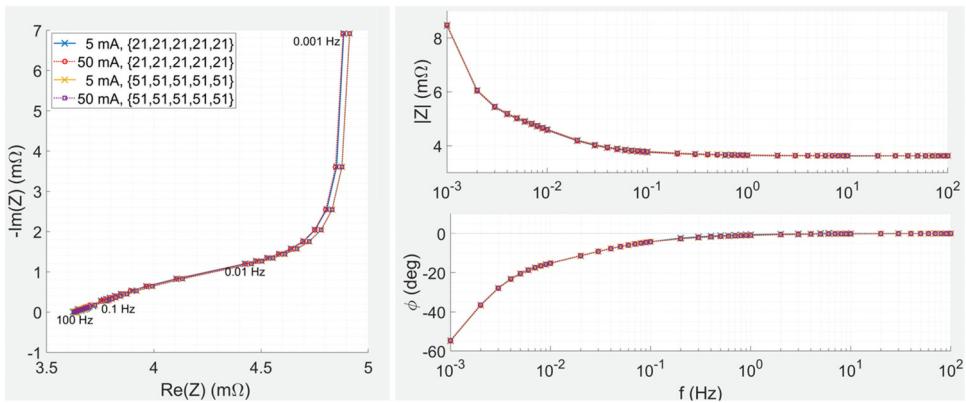


Figure 16. Nyquist (left) and Bode (right) plots of the cell impedance calculated by simulating the EIS measurement with *LiIonCellP2D*. CPU time (units: s) for integration using Dymola 2024x installed on Microsoft Windows 11 and a Lenovo ThinkPad with an 11th Gen Intel Core i9: $0.833 + 1.01 + 1.32 + 1.26 + 1.45 = 5.88$ s for 5 mA, {21,21,21,21,21}; $1.01 + 1.35 + 1.26 + 1.47 + 1.81 = 6.90$ s for 50 mA, {21,21,21,21,21}; $9.38 + 12.0 + 10.5 + 11.9 + 14.0 = 57.8$ s for 5 mA, {51,51,51,51,51}; and $9.31 + 12.2 + 10.3 + 11.9 + 13.8 = 57.5$ s for 50 mA, {51,51,51,51,51}.

The input current is sinusoidal with zero mean ($I_{0,DC} = 0$). Simulations are performed for two different amplitudes of the cell current: $I_{0,AC} = 5$ mA and $I_{0,AC} = 50$ mA. Since the cell parameter values correspond to only one sheet and the complete battery contains 48 sheets, the amplitude of the simulated current is 5/48 mA and 50/48 mA, respectively. To analyse the dependence with the cell spatial discretization, two spatial discretizations are considered: $\{21,21,21,21,21\}$ and $\{51,51,51,51,51\}$.

Combining the two levels of these two experimental factors (sinusoidal current amplitude and spatial discretization size), four EIS analyses are simulated. The tolerance of the *dassl* algorithm implemented in *Dymola* is set to $1e-7$. The results of the simulated EIS analyses are shown in [Figure 16](#). In this experiment, the main effects of spatial discretization and current amplitude on cell impedance can be considered as significant and negligible, respectively.

The CPU time of each experimental run is given in the figure caption (as the sum of the CPU time of five simulations, one per frequency group). The main effect of the spatial discretization on the CPU time is significant. Under the given conditions, the CPU time for the spatial discretization $\{21,21,21,21,21\}$ is in the order of a few seconds and for $\{51,51,51,51,51\}$ in the order of a minute. The main effect of the current amplitude on the CPU time can be considered negligible.

7. Conclusions

A novel Modelica library named *LiIonCellP2D* has been presented. It contains a variant of the pseudo two-dimensional DFN model and supports common cell characterization techniques, including those based on current pulse trains (e.g. charge/discharge cycles at constant current, GITT and HPPC), constant-current constant-voltage cycles, and EIS.

The modelling approach adopted in *LiIonCellP2D* consists in discretizing the two spatial dimensions of the DFN model into control volumes, where mass and charge conservation is imposed. This approach does not hinder the physical interpretation of the model and facilitates the description of spatial inhomogeneities of medium properties such as the volume fractions occupied by the solid and the electrolyte, the electron and ionic conductivities, the solid particle radius and the permeability factor, which can be defined independently in each control volume.

The *LiIonCellP2D* models have been formulated to achieve numerical efficiency and robustness. Concerning the latter, discontinuities in the cell current are avoided during the analyses. Taking advantage of *Dymola*'s efficient algorithms for sparse DAE, the CPU times to run the simulations discussed in [Section 6](#) are on the order of seconds for constant current charge and discharge, constant current–constant voltage cycling, and current pulses; and on the order of 1 minute for the EIS analysis to calculate cell impedance for 46 frequencies spanning 5 decades.

The *LiIonCellP2D* library has been designed and programmed in Modelica, according to the principles of the object-oriented modelling methodology, and the physical modelling paradigm (Åström, Elmqvist, and Mattsson 1998). This has facilitated developing the models, structuring them into a well-organized model library and using them.

Disclosure statement

No potential conflict of interest was reported by the author(s).

Funding

This research was performed in the frame of the REBELION project, which is funded by the European Union's Horizon Europe research and innovation programme under grant agreement No [101104241]. Views and opinions expressed are however those of the author(s) only and do not necessarily reflect those of the European Union or CINEA. Neither the European Union nor the granting authority can be held responsible for them.

References

- Arianto, S, Yuwono R, Prihandoko B. 2016. Modeling of lithium ion battery using Modelica and Scilab/Xcos. *ECS Trans.* 73:241–248. doi:[10.1149/07301.0241ecst](https://doi.org/10.1149/07301.0241ecst).
- Arora, P, White RE, Doyle M. 1998. Capacity fade mechanisms and side reactions in lithium-ion batteries. *J. Electrochem. Soc.* 145(10):3647–3667. oct. doi:[10.1149/1.1838857](https://doi.org/10.1149/1.1838857)
- Åström, KJ, Elmqvist H, Mattsson SE. 1998. Evolution of continuous-time modeling and simulation. In: *Proceedings of the 12th European Simulation Multiconference*, Manchester, UK. p. 1–10.
- Bizeray, A. 2016. State and parameter estimation of physics-based lithium-ion battery models. Phd dissertation. University of Oxford.
- Comsol. 2024. Comsol multiphysics. <https://www.comsol.com/>
- Dandeliion Team. 2024. Dandeliion - Ultra-fast online solution to the Newman model of Li-ion battery performance. <https://www.dandeliion.com/>
- Dao, TS, Schmitke C Developing mathematical models of batteries in Modelica for energy storage applications. In: *Proceedings of the 11th International Modelica Conference*, Versailles, France; 2015. p. 469–477.
- Dassault Systèmes AB. Dymola - Dynamic modeling laboratory, full user manual. September 2023 (Dymola 2024x).
- Doyle, M. 1995. Design and simulation of lithium rechargeable batteries. Phd thesis. Berkeley: Lawrence Berkeley National Laboratory, University of California. <https://escholarship.org/uc/item/6j87z0sp>.
- Doyle, M, Fuller TF, Newman J. 1993. Modeling of galvanostatic charge and discharge of the lithium/polymer/insertion cell. *J. Electrochem. Soc.* 140(6):1526–1533. doi:[10.1149/1.2221597](https://doi.org/10.1149/1.2221597).
- Doyle, M, Newman J. 1995. The use of mathematical modeling in the design of lithium/polymer battery systems. *Electrochim. Acta.* 40(13):2191–2196. doi:[10.1016/0013-4686\(95\)00162-8](https://doi.org/10.1016/0013-4686(95)00162-8).
- Dvorak, D, Lacher H, Simic D. 2014. Thermal modeling and validation of a lithium-ion battery based on electric vehicle measurements. In: *Proceedings of the 2014 IEEE Conference on Vehicle Power and Propulsion (VPPC)*, Coimbra, Portugal. p. 1–6.
- Ecker, M, Käbitz S, Laresgoiti I, Sauer DU. 2015. Parameterization of a physico-chemical model of a lithium-ion battery - II. Model validation. *J. Electrochem. Soc.* 162(9):A1849–A1857. doi:[10.1149/2.0541509jes](https://doi.org/10.1149/2.0541509jes).
- Ecker, M, Tran TKD, Dechent P, Käbitz, S, Warnecke, A, Sauer, DU. 2015. Parameterization of a physico-chemical model of a lithium-ion battery - I. Determination of parameters. *J. Electrochem. Soc.* 162(9):A1236–A1245. doi:[10.1149/2.0551509jes](https://doi.org/10.1149/2.0551509jes).
- Fuller, T, Doyle M, Newman J. 1994. Simulation and optimization of the dual lithium ion insertion cell. *J. Electrochem. Soc.* 141:1. <https://iopscience.iop.org/article/10.1149/1.2054684>
- Gamma Technologies. GT-AutoLion. 2024. <https://www.gtisoft.com/gt-autolion/>
- Gerl, J, Janczyk L, Krüger I, Modrow, N. 2014. A Modelica based lithium ion battery model. In: *Proceedings of the 10th International Modelica Conference*, Lund, Sweden. p. 335–341.

- Groß, C, Golubkov A. **2021**. A Modelica library for thermal-runaway propagation in lithium-ion batteries. In: Proceedings of the 14th International Modelica Conference, Linköping, Sweden. p. 215–224.
- Hariharan, KS, Tagade P, Ramachandran S. **2018**. Mathematical modeling of lithium batteries: from electrochemical models to state estimator algorithms. Cham, Switzerland: Springer.
- Korotkin, I, Sahu S, O’Kane SEJ, Richardson G, Foster JM. **2021**. Dandelion v1: an extremely fast solver for the Newman model of lithium-ion battery (dis)charge. *J. Electrochem. Soc.* 168 (6):060544. jun. doi:10.1149/1945-7111/ac085f
- Lasia, A. **2014**. Electrochemical impedance spectroscopy and its applications. New York: Springer.
- Légrand, N, Raël S, Knosp B, Hinaje M, Desprez P, Lapique F. **2014**. Including double-layer capacitance in lithium-ion battery mathematical models. *J. Power Sources.* 251:370–378.
- Maplesoft. **2024**. MapleSim Battery Library. <https://www.maplesoft.com/products/toolboxes/battery/>.
- Modelon. **2024a**. Electrification library. <https://modelon.com/library/electrification-library/>
- Modelon. **2024b**. Modelon lithium ion batteries. <https://modelon.com/blog/battery-modeling-electric-vehicles-rimac/>
- O’Kane, SEJ, Ai W, Madabattula G, Alonso-Alvarez D, Timms R, Sulzer V, Edge JS, Wu B, Offer GJ, Marinescu M, et al. **2022**. Lithium-ion battery degradation: how to model it. *Phys. Chem. Chem. Phys.* 24(13):7909–7922. doi:10.1039/D2CP00417H.
- Ong, I, Newman J. **1999**. Double-layer capacitance in a dual lithium ion insertion cell. *J. Electrochem. Soc.* 146:4360–4365
- Pine, S, Choudhury B. **2020**. Battery performance optimization of an electric vehicle in Modelica. *Indian J. Nat. Sci.* 11:28691–28696.
- Qin, D, Li J, Wang T, Zhang D. **2019**. Modeling and simulating a battery for an electric vehicle based on Modelica. *Autom. Innov.* 2:169–177. doi:10.1007/s42154-019-00066-0.
- Ramadass, P, Haran B, White R, Popov BN. **2003**. Mathematical modeling of the capacity fade of Li-ion cells. *J. Power Sources.* 123(2):230–240. <https://www.sciencedirect.com/science/article/pii/S0378775303005317>
- Smith, K, Wang CY. **2006**. Solid-state diffusion limitations on pulse operation of a lithium ion cell for hybrid electric vehicles. *J. Power Sources.* 161(1):628–639. <https://www.sciencedirect.com/science/article/pii/S0378775306006161>
- Srinivasan, V, Wang CY. **2002**. Analysis of electrochemical and thermal behavior of Li-ion cells. *J. Electrochem. Soc.* 150(1):A98. <https://iopscience.iop.org/article/10.1149/1.1526512>
- Sulzer, V, Marquis S, Timms R, Robinson M, Chapman SJ. **2021**. Python battery mathematical modelling (PyBaMM). *J. Open Res. Software.* 9(1):14. doi:10.5334/jors.309.
- Thomas, KE, Darling RM, Newman J. **2021**. Mathematical modeling of lithium batteries. Lawrence Berkeley National Laboratory, University of California, Berkeley. <https://escholarship.org/uc/item/6905515d>.
- Torchio, M, Magni L, Gopaluni RB, Braatz RD, Raimondo DM. **2016**. Lionsimba: a Matlab framework based on a finite volume model suitable for Li-ion battery design, simulation, and control. *J. Electrochem. Soc.* 163(7):A1192. apr. doi:10.1149/2.0291607jes
- Uddin, K, Picarelli A. **2014**. Phenomenological Li ion battery modelling in Dymola. In: Proceedings of the 10th International Modelica Conference. p. 327–334.
- US Department of Energy. **2014**. Battery test manual for plug-in hybrid electric vehicles. The Idaho National Laboratory, U.S. Department of Energy, Vehicle Technologies Program. INL/EXT-14-32849. <https://inldigitallibrary.inl.gov/sites/sti/sti/6308373.pdf>
- West, K, Jacobsen T, Atlung S. **1982**. Modeling of porous insertion electrodes with liquid electrolyte. *J. Electrochem. Soc.* 129(7):1480. doi:10.1149/1.2124188